

MAGNETIC FIELD GENERATION IN COLLISIONLESS SHOCKS: PATTERN GROWTH AND TRANSPORT

J. TRIER FREDERIKSEN, C. B. HEDEDAL, T. HAUGBØLLE, AND Å. NORDLUND

Department of Astrophysics, Niels Bohr Institute, Juliane Maries Vej 30, 2100 København Ø, Denmark; trier@astro.ku.dk

Received 2003 August 7; accepted 2004 March 23; published 2004 May 13

ABSTRACT

We present results from three-dimensional particle simulations of collisionless shock formation, with relativistic counterstreaming ion-electron plasmas. Particles are followed over many skin depths downstream of the shock. Open boundaries allow the experiments to be continued for several particle crossing times. The experiments confirm the generation of strong magnetic and electric fields by a Weibel-like kinetic streaming instability and demonstrate that the electromagnetic fields propagate far downstream of the shock. The magnetic fields are predominantly transversal and are associated with merging ion current channels. The total magnetic energy grows as the ion channels merge and as the magnetic field patterns propagate downstream. The electron populations are quickly thermalized, while the ion populations retain distinct bulk speeds in shielded ion channels and thermalize much more slowly. The results help reveal processes of importance in collisionless shocks and may help to explain the origin of the magnetic fields responsible for afterglow synchrotron/jitter radiation from gamma-ray bursts.

Subject headings: acceleration of particles — gamma rays: bursts — instabilities — magnetic fields — plasmas

1. INTRODUCTION

The existence of a strong magnetic field in the shocked external medium is required in order to explain the observed radiation in gamma-ray burst afterglows as synchrotron radiation (e.g., Panaitescu & Kumar 2002). Nearly collisionless shocks, with synchrotron-type radiation present, are also common in many other astrophysical contexts, such as in supernova shocks and in jets from active galactic nuclei. At least in the context of gamma-ray burst afterglows the observed synchrotron radiation requires the presence of a stronger magnetic field than can easily be explained by just compression of a magnetic field already present in the external medium.

Medvedev & Loeb (1999) showed through a linear kinetic treatment how a two-stream magnetic instability—a generalization of the Weibel instability (Weibel 1959; Yoon & Davidson 1987)—can generate a strong magnetic field (ϵ_B , defined as the ratio of magnetic energy to total kinetic energy, is 10^{-5} to 10^{-1} of equipartition value) in collisionless shock fronts (see also the discussion in Rossi & Rees 2003). We note in passing that this instability is well known in other plasma physics disciplines, e.g., laser-plasma interactions (Yang et al. 1993; Califano et al. 1998), and has been applied in the context of pulsar winds by Kazimura et al. (1998).

Using three-dimensional particle-in-cell simulations to study relativistic collisionless shocks (where an external plasma impacts the shock region with a bulk Lorentz factor $\Gamma = 5\text{--}10$), Frederiksen et al. (2003), Nishikawa et al. (2003), and Silva et al. (2003) investigated the generation of magnetic fields by the two-stream instability. In these first studies the growth of the transverse scales of the magnetic field was limited by the dimensions of the computational domains. The durations of the Nishikawa et al. (2003) experiments were less than particle travel times through the experiments, while Silva et al. (2003) used periodic boundary conditions in the direction of streaming. Further, Frederiksen et al. (2003) and Nishikawa et al. (2003) used electron-ion (e^-p) plasmas, while experiments reported on by Silva et al. (2003) were done with e^-e^+ pair plasmas.

Here, we report on three-dimensional particle-in-cell simulations of relativistically counterstreaming e^-p plasmas. Open boundaries are used in the streaming direction, and experiment

durations are several particle crossing times. Our results can help reveal the most important processes in collisionless shocks and help explain the observed afterglow synchrotron radiation from gamma-ray bursts. We focus on the earliest development in shock formation and field generation. Late stages in shock formation will be addressed in successive work.

2. SIMULATIONS

Experiments were performed using a self-consistent three-dimensional electromagnetic particle-in-cell code originally developed for simulating reconnection topologies (Hesse et al. 1999), redeveloped by the present authors to obey special relativity and to be second-order accurate in both space and time.

The code solves Maxwell's equations for the electromagnetic field with continuous sources, with fields and field source terms defined on a staggered three-dimensional Yee lattice (Yee 1966). The sources in Maxwell's equations are formed by weighted averaging of particle data to the field grid, using quadratic spline interpolation. Particle velocities and positions are defined in continuous $(\mathbf{r}, \gamma\mathbf{v})$ -space, and particles obey the relativistic equations of motion.

The grid size used in the main experiment was $(x, y, z) = 200 \times 200 \times 800$, with 25 particles per cell, for a total of 8×10^8 particles, with ion-to-electron mass ratio $m_i/m_e = 16$. To adequately resolve a significant number of electron and ion skin depths (δ_e and δ_i), the box size was chosen such that $L_{x,y} = 10\delta_i \sim 40\delta_e$ and $L_z \sim 40\delta_i \sim 160\delta_e$. Varying aspect and mass ratios were used in complementary experiments.

Two counterstreaming—initially quasi-neutral and cold—plasma populations are simulated. At the two-stream interface (smoothed around $z = 80$), a plasma ($z < 80$) streaming in the positive z -direction, with a bulk Lorentz factor $\Gamma = 3$, hits another plasma ($z \geq 80$) at rest in our reference frame. The latter plasma is denser than the former by a factor of 3. Experiments have been run with both initially sharp and initially smooth transitions, with essentially the same results. The long simulation time gradually allows the shock to converge toward self-consistent jump conditions. Periodic boundaries are imposed in the x - and y -directions, while the boundaries at $z = 0$ and 800 are open, with layers absorbing transverse electro-

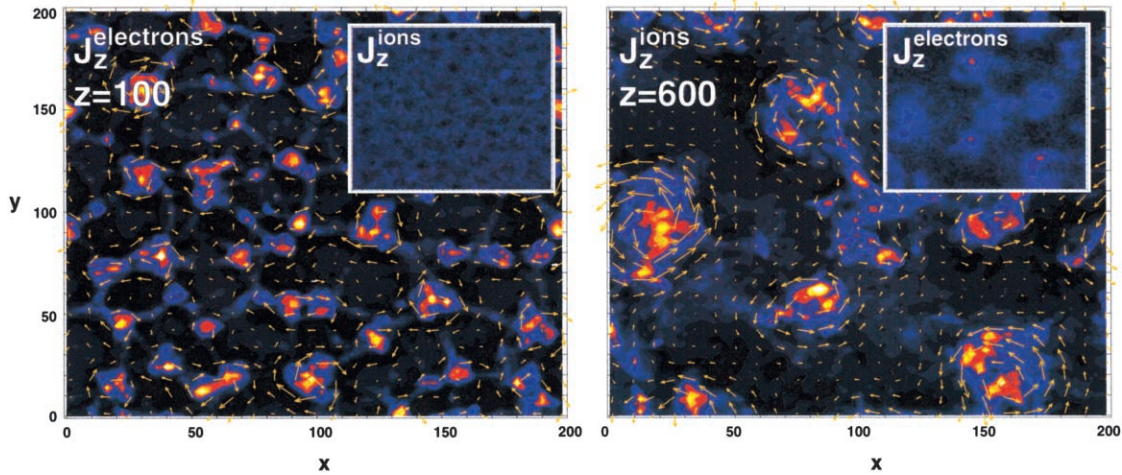


FIG. 1.—*Left*: Longitudinal electron current density through a transverse cut at $z = 100$, with a small inset showing the ion current in the same plane. *Right*: Ion current at $z = 600 = 30\delta_e$, with the small inset now instead showing the electron current. The arrows represent the transverse magnetic field. Both panels are from time $t = 1200$.

magnetic waves. Inflow conditions at $z = 0$ are fixed, with incoming particles supplied at a constant rate and with uniform speed. At $z = 800$ there is free outflow of particles. The maximum experiment duration is $480\omega_{pe}^{-1}$ (where ω_{pe} is the electron plasma frequency), sufficient for propagating $\Gamma \approx 3$ particles 2.8 times through the box.

3. RESULTS AND DISCUSSIONS

The extended size and duration of these experiments make it possible to follow the two-stream instability through several stages of development: first exponential growth, then nonlinear saturation, followed by pattern growth and downstream advection. We identify the mechanisms responsible for these stages below.

3.1. Magnetic Field Generation, Pattern Growth, and Field Transport

Encountering the shock front, the incoming electrons are rapidly (being lighter than the ions) deflected by field fluctuations growing because of the two-stream instability (Medvedev & Loeb 1999). The initial perturbations grow nonlinear as the deflected electrons collect into first caustic surfaces and then current channels (Fig. 1). Both streaming and rest-frame electrons are deflected, by arguments of symmetry.

In accordance with Ampere’s law the current channels are surrounded by approximately cylindrical magnetic fields (il-

lustrated by arrows in Fig. 1), causing mutual attraction between the current channels. The current channels thus merge in a race where larger electron channels consume smaller neighboring channels. In this manner, the transverse magnetic field grows in strength and scale downstream. This continues until the fields grow strong enough to deflect the much heavier ions into the magnetic voids between the electron channels. The ion channels are then subjected to the same growth mechanism as the electrons. When ion channels grow sufficiently powerful, they begin to experience Debye shielding by the electrons, which by then have been significantly heated by scattering on the increasing electromagnetic field structures. The two electron populations, initially separated in γv -space, merge to a single population in approximately $20\delta_e$ ($z = 80$ – 200), as seen in Figure 6. The same trend is seen for the ions, albeit at a rate slower in proportion to m_i/m_e .

The Debye shielding quenches the electron channels, while at the same time supporting the ion channels; the large random velocities of the electron population allow the concentrated ion channels to keep sustaining strong magnetic fields. Figure 1 shows the highly concentrated ion currents, the more diffuse—and shielding—electron currents, and the resulting magnetic field. The electron and ion channels are further illustrated in Figure 2. Note the limited z -extent of the electron current channels, while the ion current channels extend throughout the length of the box, merging to form larger scales downstream. Because of the longitudinal current channels the magnetic field is predominantly transversal; we find $|B_z|/|B_{\text{tot}}| \sim 10^{-1}$ to 10^{-2} .

Figure 3 shows the temporal development of the transverse magnetic field scales around $z = 250$. The power spectra follow power laws, with the largest scales growing with time. The dominant scales at these z are of the order of δ_i at early times. Later they become comparable to $L_{x,y}$. Figure 4 captures this scaling behavior as a function of depth for $t = 2400$.

The time evolutions of the electric and magnetic field energies are shown in Figure 5. Seeded by fluctuations in the fields, mass, and charge density, the two-stream instability initially grows superlinearly ($t = 80$ – 100), reflecting approximate exponential growth in a small subvolume. Subsequently the total magnetic energy grows more linearly, reflecting essentially the increasing volume filling factor as the nonlinearly saturated magnetic field structures are advected downstream.

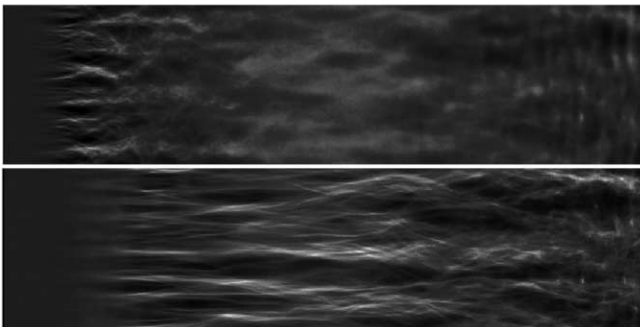


FIG. 2.—Electron (*top*) and ion (*bottom*) currents, averaged over the x -direction, at time $t = 1200$.

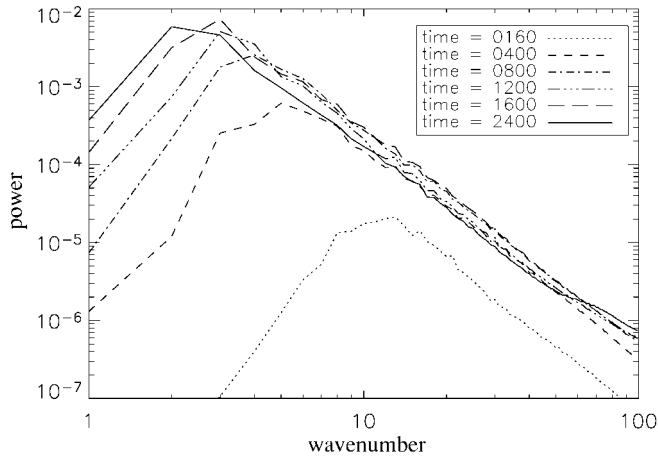


FIG. 3.—Power spectrum of B_{\perp} for $z = 250$ at different times.

At $t \approx 1100$ the slope drops off because of advection of the generated fields out of the box. The continued slow growth, for $t > 1100$, reflects the increase of the pattern size with time (cf. Fig. 3). A larger pattern size corresponds to, on the average, a larger mean magnetic energy, since the total electric current is split up into fewer but stronger ion current channels. The magnetic energy scales with the square of the electric current, which in turn grows in inverse proportion to the number of current channels. The net effect is that the mean magnetic energy increases accordingly.

The magnetic energy density keeps growing throughout our experiment, even though the duration of the experiment ($480\omega_{pe}^{-1}$) significantly exceeds the particle crossing time and also exceeds the advection time of the magnetic field structures through the box. This is in contrast to the results reported by Silva et al. (2003), where the magnetic energy density drops back after about $(10\text{--}30)\omega_{pe}^{-1}$. It is indeed obvious from the preceding discussion that the ion-electron asymmetry is essential for the survival of the current channels.

From the requirement that the total plasma momentum should be conserved, the (electro)magnetic field produced by the two-stream instability acquires part of the z -momentum lost by the two-stream population in the shock; this opens the possibility that magnetic field structures created in the shock migrate downstream of the shock and thus carry away some of the momentum impinging on the shock. Our experiments show that this does indeed happen; the continuous injection of momentum transports the generated field structures downstream

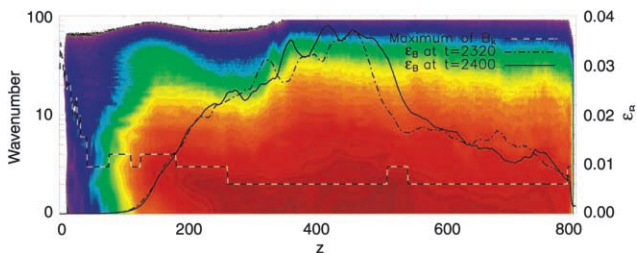


FIG. 4.—Relative electromagnetic energy density ϵ_B . The contour color plot shows the power in the transverse magnetic field through the box distributed on spatial Fourier modes at $t = 2400$, with the dotted line marking the wavenumber with maximum power. Superposed is the spatial distribution of ϵ_B , averaged across the beam, at $t = 2320$ (dash-dotted line) and $t = 2400$ (solid line), highlighting how electromagnetic fields are advected down through the box.

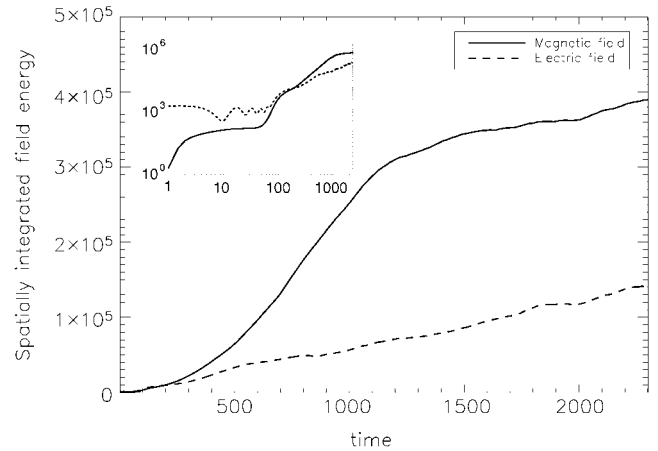


FIG. 5.—Total magnetic (solid line) and electric (dashed line) energy in the box as a function of time. The inset shows a log-log plot of the same data.

at an accelerated advection speed. The dragging of field structures through the dense plasma acts to transfer momentum between the in-streaming and the shocked plasmas.

3.2. Thermalization and Plasma Heating

At late times the entering electrons are effectively scattered and thermalized: The magnetic field isotropizes the velocity distribution, whereas the electric field generated by the e^-p charge separation acts to thermalize the populations. Figure 6 shows that this happens over the ~ 20 electron skin depths from around $z = 80\text{--}200$. The ions are expected to also thermalize, given sufficient space and time. This fact leaves the massive ion bulk momentum constituting a vast energy reservoir for further electron heating and acceleration. Also seen in Figure 6, the ions' beams stay clearly separated in phase space and are only slowly broadened (and heated).

We do not see indications of a superthermal tail in the heated electron distributions, and there is thus no sign of second-order Fermi acceleration in the experiment presented in this Letter. Nishikawa et al. (2003) and Silva et al. (2003) reported acceleration of particles in experiments similar to the current experiment, except for more limited sizes and durations, and the use of an e^-e^+ plasma (Silva et al. 2003). On closer ex-

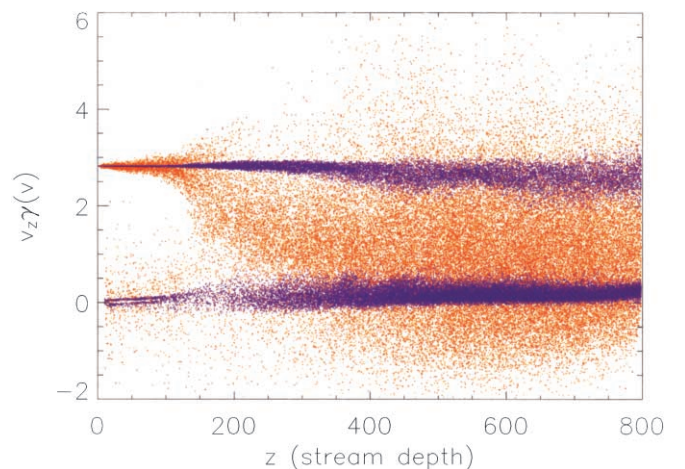


FIG. 6.—Thermalization and longitudinal acceleration, illustrated by scatter plots of the electron (orange) and ion (blue) populations. Note the backscattered electron population [$v_z \gamma(v) < 0$].

amination of the published results it appears that there is no actual disagreement regarding the absence of accelerated particles. Nishikawa et al. (2003) refer to transversal velocities of the order of $0.2c$ (their Fig. 3*b*) at a time where our experiment shows similar transversal velocities (cf. Fig. 6) that later develop a purely thermal spectrum. Silva et al. (2003) refer to transversal velocity amplitudes up to about $0.8c$ (their Fig. 4), or $v\gamma \sim 2$, with a shape of the distribution function that appears to be compatible with thermal. In comparison, the electron distribution illustrated by the scatter plot in Figure 6 covers a similar interval of $v\gamma$, with distribution functions that are close to (Lorentz-boosted) relativistic Maxwellians. Thus, there is so far no compelling evidence for nonthermal particle acceleration in experiments with no imposed external magnetic field. Thermalization is a more likely cause of the increases in transversal velocities.

Frederiksen et al. (2003) reported evidence for particle acceleration, with electron gammas up to ~ 100 , in experiments with an external magnetic field present in the upstream plasma. This is indeed a more promising scenario for particle acceleration experiments (although in the experiments by Nishikawa et al. 2003, results with an external magnetic field were similar to those without). Figure 6 shows the presence of a population of backscattered electrons ($v\gamma < 0$). In the presence of an external magnetic field in the in-streaming plasma, this possibly facilitates Fermi acceleration in the shock.

4. CONCLUSIONS

The experiment reported on here illustrates a number of fundamental properties of relativistic collisionless shocks:

1. Even in the absence of a magnetic field in the upstream plasma, a small-scale, fluctuating, and predominantly transversal magnetic field is unavoidably generated by a two-stream instability reminiscent of the Weibel instability. In the current experiment the magnetic energy density reaches a few percent of the energy density of the incoming beam.

2. In the case of an e^-p plasma the electrons are rapidly thermalized, while the ions form current channels that are the sources of deeply penetrating magnetic field structures. The channels merge in the downstream direction, with a corresponding increase of the average magnetic energy with shock depth. This is expected to continue as long as a surplus of bulk relative momentum remains in the counterstreaming plasmas.

3. The generated magnetic field patterns are advected downstream at speeds intermediate of the incoming plasma and the rest-frame plasma. The electromagnetic field structures thus provide scattering centers that interact with both the fast incoming plasma and the plasma that is initially at rest. As a result the electron populations of both components quickly thermalize and form a single Lorentz-boosted thermal electron population. The two ion populations merge much more slowly, with only gradually increasing ion temperatures.

4. The observed strong turbulence in the field structures at the shocked streaming interface provides a promising environment for particle acceleration.

We emphasize that quantification of the interdependence and development of ϵ_U and ϵ_B is accessible by means of such experiments as reported on here. Rather than devising abstract scalar parameters ϵ_B and ϵ_U , which may be expected to depend on shock depth, media densities, etc., a better approach is to compute synthetic radiation spectra directly from the models and then apply scaling laws to predict what would be observed from corresponding real supernova remnants and gamma-ray burst afterglow shocks.

We are grateful to Michael Hesse/GSFC for generously providing the original particle-in-cell code and for helpful discussions on the implementation and on numerical issues in particle simulations. Computer time was provided by the Danish Center for Scientific Computing.

REFERENCES

- Califano, F., Pegoraro, S., Bulanov, V., & Mangeney, A. 1998, *Phys. Rev. E*, 57, 7048
- Frederiksen, J. T., Hededal, C. B., Haugbølle, T., & Nordlund, Å. 2003, preprint (astro-ph/0303360)
- Hesse, M., Schindler, K., Birn, J., & Kuznetsova, M. 1999, *Phys. Plasmas*, 6, 1781
- Kazimura, Y., Sakai, J. I., Neubert, T., & Bulanov, S. V. 1998, *ApJ*, 498, L183
- Medvedev, M. V., & Loeb, A. 1999, *ApJ*, 526, 697
- Nishikawa, K.-I., Hardee, P., Richardson, G., Preece, R., Sol, H., & Fishman, G. J. 2003, *ApJ*, 595, 555
- Panaitescu, A., & Kumar, P. 2002, *ApJ*, 571, 779
- Rossi, E., & Rees, M. J. 2003, *MNRAS*, 339, 881
- Silva, L. O., Fonseca, R. A., Tonge, J. W., Dawson, J. M., Mori, W. B., & Medvedev, M. V. 2003, *ApJ*, 596, L121
- Weibel, E. S. 1959, *Phys. Rev. Lett.*, 2, 83
- Yang, T.-Y. B., Gallant, Y., Arons, J., & Langdon, A. B. 1993, in *Isolated Pulsars*, ed. K. A. Rippen, R. I. Epstein, & C. Ho (Cambridge: Cambridge Univ. Press), 357
- Yee, K. S. 1966, *IEEE Trans. Antennas Propag.*, 14, 302
- Yoon, P. H., & Davidson, R. C. 1987, *Phys. Rev. A*, 35, 2718